Deep-Sea Research I 107 (2016) 9–21

Contents lists available at ScienceDirect

Deep-Sea Research I

journal homepage: www.elsevier.com/locate/dsri

The decomposition of the Faroe-Shetland Channel water masses using Parametric Optimum Multi-Parameter analysis

C. McKenna [a], B. Berx [b,*], W.E.N. Austin [a,c]

[a] School of Geography and Geosciences, University of St Andrews, St Andrews, Fife KY16 9AL, Scotland
[b] Marine Scotland Science, Scottish Government, Marine Laboratory, 375 Victoria Road, Aberdeen AB11 9 DB, Scotland
[c] Scottish Marine Institute, Scottish Association for Marine Science, Oban PA37 1QA, Scotland

ARTICLE INFO

Article history:
Received 16 January 2015
Received in revised form
26 October 2015
Accepted 31 October 2015
Available online 9 November 2015

Keywords:
Faroe-Shetland Channel
North Atlantic
Water mass mixing
Mixing models
POMP analysis
$\delta^{18}O$
Nutrients

ABSTRACT

The Faroe-Shetland Channel (FSC) is an important conduit for the poleward flow of Atlantic water towards the Nordic Seas and, as such, it plays an integral part in the Atlantic's thermohaline circulation. Mixing processes in the FSC are thought to result in an exchange of properties between the channel's inflow and outflow, with wider implications for this circulation; the nature of this mixing in the FSC is, however, uncertain. To constrain this uncertainty, we used a novel empirical method known as Parametric Optimum Multi-Parameter (POMP) analysis to objectively quantify the distribution of water masses in the channel in May 2013. This was achieved by using a combination of temperature and salinity measurements, as well as recently available nutrient and $\delta^{18}O$ measurements. The outcomes of POMP analysis are in good agreement with established literature and demonstrate the benefits of representing all five water masses in the FSC. In particular, our results show the recirculation of Modified North Atlantic Water in the surface layers, and the pathways of Norwegian Sea Arctic Intermediate Water and Norwegian Sea Deep Water from north to south for the first time. In a final step, we apply the mixing fractions from POMP analysis to decompose the volume transport through the FSC by water mass. Despite a number of caveats, our study suggests that improved estimates of the volume transport of Atlantic inflow towards the Arctic and, thus, the associated poleward fluxes of salt and heat are possible. A new prospect to more accurately monitor the strength of the FSC branch of the thermohaline circulation emerges from this study.

1. Introduction

The poleward flow of warm and saline Atlantic water through the Faroe-Shetland Channel (FSC) accounts for a large fraction of the total Atlantic inflow into the Nordic Seas (~2.7 Sv; Berx et al., 2013). This is slightly less than the inflow over the Iceland-Faroe Ridge (~3.8 Sv), and significantly greater than that through the Denmark Strait (~0.8 Sv) (Østerhus et al., 2005). As such, the FSC is an important conduit for the poleward transport of salt, heat and nutrients, which, for example, creates favourable conditions for the economically important fish stocks in the Nordic Seas (Larsen et al., 2012). Furthermore, this transport of salt also enhances intermediate and deep water formation in the Arctic (Hansen et al., 2003). These intermediate and deep waters then flow back towards the south via the same pathways, transporting a total ~5.6 Sv of water into the North Atlantic (Sherwin et al., 2008a), of which ~2.2 Sv overflows through the FSC (Hansen and Østerhus, 2007; Sherwin et al., 2008a). The FSC is therefore an integral gateway to the present operation of the global thermohaline circulation and, as such, research into the nature of mixing and circulation within the channel is important.

Monitoring of the properties (temperature and salinity) of oceanic water masses in the FSC started in the early 20th century (Dickson, 1903). However, a programme of regularly repeated surveys was only established from the 1970s. From 2000, the analysis of samples for nutrient concentrations was added. These observations have focussed on two hydrographic sections across the FSC: the Nolso-Flugga (NOL) and Fair Isle-Munken (FIM) sections (Fig. 1). Through these measurements, it is now well-established that five water masses of contrasting origin flow through the FSC, as summarised by Hansen and Østerhus (2000): North Atlantic Water (NAW), Modified North Atlantic Water (MNAW), Modified East Icelandic Water (MEIW), Norwegian Sea Arctic Intermediate Water (NSAIW) and Norwegian Sea Deep Water (NSDW). These water masses are distinguished by distinct temperature and salinity characteristics (Table 1), which have been used to trace their presence or absence in the channel (Martin, 1993; Turrell et al., 1999; Borenäs et al., 2001).

* Corresponding author.
E-mail address: b.berx@marlab.ac.uk (B. Berx).

http://dx.doi.org/10.1016/j.dsr.2015.10.013

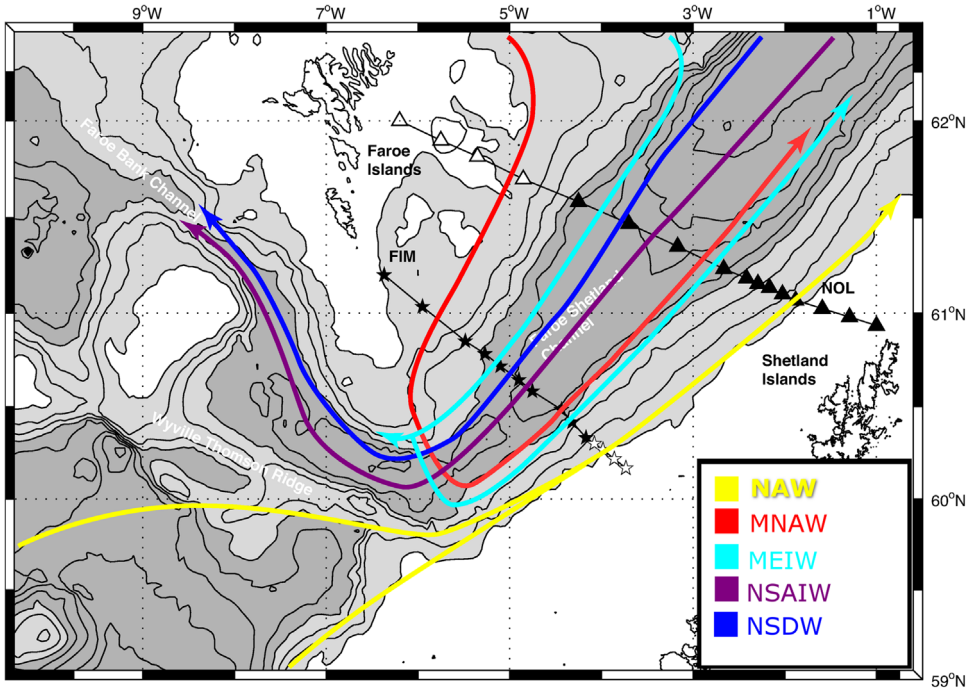

Fig. 1. Map of the Faroe-Shetland Channel showing two standard hydrographic sections: Nolso-Flugga (NOL; triangles), and Fair Isle-Munken (FIM; stars). General circulation of the 5 main water masses is also shown (NAW = North Atlantic Water; MNAW = Modified North Atlantic Water; MEIW = Modified East Icelandic Water; NSAIW = Norwegian Sea Arctic Intermediate Water; NSDW = Norwegian Sea Deep Water). Open symbols show where SWT definitions were determined for MNAW and NAW (see text).

Table 1
Source Water Types (SWTs) for each water mass used in the POMP analysis (no brackets). In brackets, reference SWT ranges taken from literature and databases for comparison. In the bottom row, uncertainties in each hydrographic property used for the weighting. Phosphate, nitrate and silicate reference SWT ranges for the MEIW, NSAIW and NSDW (except for the NSDW phosphate range) were estimated from data obtained from the northern boundary of the FSC to minimise the influence of mixing. $\delta^{18}O$ reference SWT ranges for the NAW were estimated from data obtained from the Rockall Trough; from the Iceland Basin and areas southwest of the Rockall Trough for the MNAW; from around the northern coast of Iceland for the MEIW; from the Lofoten and Norwegian Basins for the NSAIW; and from the Eurasian and Greenland Basins for the NSDW.

	Potential temp. (°C)	Salinity	Phosphate (μmol/l)	Nitrate (μmol/l)	Silicate (μmol/l)	$\delta^{18}O$ (‰)
NAW	10.15 (9.5–10.5)[a]	35.42 (35.35–35.45)[a]	0.65 (0.6–1.1)[c]	10.21 (9–16)[c]	3.18 (2.5–7.5)[c]	0.49 (0.38–0.5)[f]
MNAW	8.17 (7–8.5)[a]	35.27 (35.1–35.3)[a]	0.77 (0.6–1.1)[c]	12.41 (9–16)[c]	4.84 (2.5–7.5)[c]	0.42 (0.19–0.42)[f]
MEIW	2.63 (2–4.5)[b]	34.89 (34.76–34.99)[b]	0.88 (0.85–0.97)[d]	13.2 (12.1–13.2)[d]	6.29 (5.8–7.3)[d]	0.24 (0.07–0.29)[f]
NSAIW	−0.17 (−0.5–0.5)[a,b]	34.90 (34.89–34.91)[b]	0.96 (0.9–1.1)[d]	14.11 (13.2–14.9)[d]	7.60 (9.6–12.3)[d]	0.30 (0.14–0.42)[f]
NSDW	−0.79 (< −0.5)[a]	34.91 (=34.91)[a]	1.02 (0.8–1.1)[d]	15.00 (9.6–14.8)[d]	11.77 (=11.5)[e]	0.26 (0.13–0.40)[f]
Uncertainty	0.5	0.024	0.12	1.95	1.16	0.12

[a] Hansen and Østerhus (2000);
[b] Borenäs et al. (2001);
[c] Johnson et al. (2013);
[d] World Ocean Atlas 2013 (Garcia et al. 2014);
[e] van Bennekom (1985);
[f] Global Seawater Oxygen-18 Database (version 1.21) (Schmidt et al., 1999).

While temperature–salinity (T–S) plots have been useful for identifying both spatial and temporal variability in the water masses, they cannot always explain its cause. For instance, MEIW is identified in T–S space by a convex curve shape. Seasonal variations in the degree of curve convexity have, thus, implied that the MEIW is only seasonally present in the FSC (Borenäs et al., 2001). However, while an absence of convexity may imply an absence of MEIW, it may equally imply intense mixing, or a change in MEIW's source water properties. Similarly, while it is thought that MNAW and MEIW partially recirculate between NOL and FIM (Dooley and Meincke, 1981; van Aken, 1988; Sherwin et al., 1999, 2008b), it is not known exactly how much recirculation occurs, because recirculation affects T–S curve shape in a similar manner to mixing. As such, mixing relationships between the FSC water masses are currently uncertain. An improved understanding of the mixing relationships is necessary, however, to fully characterize the exchange of heat, salt and nutrients between the FSC inflow and overflow. The nature of this mixing determines whether there is a potential for long term trends in the properties of one water mass to propagate into another, with wider implications for the thermohaline circulation (Hosegood et al., 2005). Indeed, mixing in the FSC between freshening Atlantic waters and intermediate waters may have enhanced wide-scale freshening of the northern North Atlantic in the 1960s, 70s and 80s, which is thought to have weakened convective overturning (Dickson et al., 1988). As global climate models have simulated a future weakening of the thermohaline circulation in response to greenhouse gas forcing (Gregory et al., 2005), it is thus vital that we understand how mixing in the FSC might act as a positive feedback mechanism in this globally significant process.

Potential mixing relationships have been identified in the FSC through the examination of mixing mechanisms (Hosegood and van Haren, 2004; Sherwin et al., 2006; Hall et al., 2011), but this can only yield qualitative results and does not quantify the mixing that occurs. However, a number of empirical "black box" mixing models do exist, and these can be used to objectively calculate mixing fractions (the percentage of each water mass at each point in the channel) with relative ease. The simplest of these, the three-point mixing model (Hermann, 1967), has already been successfully applied to the FSC (Turrell et al., 1999; Hansen et al., 2003;

Hughes et al., 2006). However, this method uses only two parameters (usually temperature and salinity) and, therefore, cannot represent more than three of the FSC water masses without compromising the statistical significance of the solution. The more complex method of Optimum Multi-Parameter (OMP) analysis (Tomczak and Large, 1989) overcomes this problem through using additional parameters - for example, nutrient concentrations. Despite this development, however, it has only been used to represent three water masses in the FSC (Borenäs et al., 2001). This method was extended by de Brauwere et al. (2007)to include a parameterisation of the mixing fractions as a function of position, known as Parametric Optimum Multi-Parameter (POMP) analysis. This advanced method places a further constraint on the problem, thereby reducing the number of unknown variables. Furthermore, the parameterisation reduces the method's sensitivity to stochastic errors, consequently increasing the accuracy of the mixing fractions obtained.

Thus, the novel method of POMP analysis gives us an opportunity to calculate mixing fractions for all five of the FSC water masses for the first time (Hansen and Østerhus, 2000), which will be the main focus of this paper. This will be achieved by using a combination of conductivity temperature depth (CTD) data, and recently available nutrient and stable oxygen isotope ($\delta^{18}O$) data. Indeed, nutrients have often been used in past OMP-like analyses (Klein and Tomczak, 1994; Maamaatuaiahutapu et al., 1994; Larqué et al., 1997) and $\delta^{18}O$ could provide a particularly powerful constraint as it is quasi-conservative (Meredith et al., 1999; Frew et al., 2000; Austin and Inall, 2002). However, despite the considerable potential of $\delta^{18}O$ and nutrient concentrations, no previous studies have used the former as a tracer of water masses in the FSC and there has been limited use of the latter as a water mass tracer. Therefore, our first aim is to establish the characteristics of each of the FSC water masses. Following this, we will use different combinations of nutrient and $\delta^{18}O$ data to determine the optimum data combination for performing POMP analysis in the FSC. The final results using this optimum combination will then be used to investigate mixing relationships between the water masses. Finally, POMP-determined fractions will be used to decompose the volume transport by water mass. This has the potential to improve estimates of the volume transport of Atlantic inflow towards the Arctic and, thus, could also improve estimates of the associated poleward fluxes of salt and heat.

2. Methods

2.1. Data

The data we present here were collected on the Fair Isle – Munken (FIM) and Nolso – Flugga (NOL) standard hydrographic sections during research cruises aboard MRV *Scotia* between May 2009 and May 2013. In this paper, mixing fractions were calculated for data collected in May 2013, but data from the period 2009–2012 were used in the definition of input parameters for the POMP method. These hydrographic sections have 14 and 16 stations, respectively, where temperature and conductivity profiles are collected using a Seabird SBE-911plus CTD sensor. Fig. 1 shows station locations on both sections. Water samples were collected at standard depths using Niskin bottles and were analysed for salinity, oxygen isotopes and nutrient concentrations. Salinity was determined from these samples using a Guildline Portasal, calibrated against IAPSO Standard Seawater (provided by OSIL).

Water samples were also analysed for Dissolved Inorganic Phosphorous (DIP), dissolved silicate (DSi) and total oxidised nitrogen (TOxN: nitrate plus nitrite). The analysis was performed using colorimetric methods on a Bran and Luebbe QuAAtro continuous flow analysis system, based on Armstrong et al. (1967) for TOxN, Murphy and Riley (1962) for DIP, and Koroleff (1971) for DSi. Data quality assurance was achieved through participation in the QUASIMEME programme (Quality Assurance of Information for Marine Environmental Monitoring in Europe).

During the May 2013 cruise, water samples were collected in addition to salinity and nutrient samples from five stations across the FIM section, with a vertical spacing of 100 m at the channel's centre and every few 100 m otherwise. Archive water samples were also available from cruises in May and October 2009–2012, which were collected every few 100 m from FIM01 and FIM06 every year, and every 100 m from FIM05 and NOL04 in October 2012. These were sealed in air-tight glass water bottles and analysed later for $\delta^{18}O$ content on a Finnegan Delta plus XP gas source mass spectrometer, coupled to a gasbench II preparation system, at the School of Geography and Geosciences, University of St Andrews. The $\delta^{18}O$ measurements were based on 1 ml volumes, determined via CO_2 equilibration. The mean precision of the triplicate analysis was $\pm 0.04‰$ relative to Vienna Standard Mean Ocean Water (VSMOW2) (see Table S1 in Supplementary Items for full details of reporting standards). 10 samples were measured in triplicate and three internal standard waters (calibrated to VSMOW2) were analysed every 10 samples.

2.2. POMP analysis

OMP and POMP analysis are based on the assumption that hydrographic properties at each point in the water column arise from the mixing of a number, n_s, of source water masses. In classical OMP analysis (Tomczak and Large, 1989), mixing equations of the form below are constructed for each property – say temperature, T – at each location, k:

$$T(k) = \sum_{i=1}^{n_s} x_i(k) T_i + e_T(k), \tag{1}$$

where $T(k)$ is the observed temperature at k (known), $x_i(k)$ is the fraction of the ith source water at k(unknown), T_i is the characteristic temperature of the ith source water (known and independent of k) and $e_T(k)$ is the error at k due to random noise. If there are n_v hydrographic properties, the mixing equations for each property at each location k can be combined into the following matrix equation:

$$\boldsymbol{y_k} = \boldsymbol{S} \bullet \boldsymbol{x_k} + \boldsymbol{e_k},$$

where $\boldsymbol{y_k}$ is a $(n_v \times 1)$ vector containing the measurements of each property at k, $\boldsymbol{S}$ is a $(n_v \times n_s)$ matrix containing the characteristic source water properties (independent of k), $\boldsymbol{x_k}$ is a $(n_s \times 1)$ vector containing the fraction of each source water at k and $\boldsymbol{e_k}$ is a vector containing the error in each property at k. The matrix equations for each location k are then combined into a single matrix equation for all N locations:

$$\boldsymbol{Y} = \boldsymbol{S} \bullet \boldsymbol{X} + \boldsymbol{E}, \tag{2}$$

where $\boldsymbol{Y}$ is a $(n_v \times N)$ matrix containing the measurements for all N, $\boldsymbol{S}$ is the same as before, $\boldsymbol{X}$ is a $(n_s \times N)$ matrix containing the mixing fractions for all N and $\boldsymbol{E}$ is a matrix containing the errors for all N. The mixing equations contained in Eq. (2) are then solved simultaneously to optimise the mixing fractions, x_i, subject to the constraint of the mass balance equation, $x_1(k)+x_2(k)+\ldots+x_{n_S}(k)=1$. Thus, applying the OMP method yields one set of mixing fractions at each location, k.

POMP analysis uses mixing equations of a similar form to Eq. (1), but instead describes the fraction fields using a continuous function. This function is two-dimensional in space and is written in terms of longitude, l, and depth, z. Thus, instead of yielding a

discrete fraction field, POMP analysis yields a fraction field that is a continuous function of position. This results in smoother fractions that are less sensitive to noise and, thus, more robust. Technically, this is done by parameterising the fractions of each source water mass, x_i, by a number, n_B, of two-dimensional basis splines, or B-splines, $B(l, z)$:

$$x_i(l, z) = \sum_{b=1}^{n_B} c_{i,b} B_b(l, z), \tag{3}$$

where each $c_{i,b}$ is a constant co-efficient for each spline for the ith source water mass. This expression replaces x_i in Eq. (1). The B-splines are formed by combining two sets of one-dimensional basis functions:

$$B_b(l, z) = N_p(l) M_q(z),$$

where $p = 1 \ldots n_l$ and $q = 1 \ldots n_z$. The N's are of order k_l and the M's are of order k_z. N and M do not pass through the data-points but through a number (n_l and n_z respectively) of knots that are positioned uniformly across the field area. Our choice of n_l, n_z, k_l and k_z will be discussed in Section 2.4.

We can now finally express the matrix form of the mixing equations used by the POMP method. Eq. (3) can be expressed in matrix form as:

$$\boldsymbol{X} = \boldsymbol{C} \bullet \boldsymbol{B}^{\boldsymbol{T}},$$

where $\boldsymbol{C}$ is a ($n_s \times n_B$) matrix containing the spline coefficients, $\boldsymbol{B}$ is a ($N \times n_B$) matrix containing the B-splines and $\boldsymbol{B}^{\boldsymbol{T}}$ is its transpose. Thus, Eq. (2) becomes:

$$\boldsymbol{Y} = \boldsymbol{S} \bullet \boldsymbol{C} \bullet \boldsymbol{B}^{\boldsymbol{T}} + \boldsymbol{E} \tag{4}$$

Further details of the POMP method can be found in de Brauwere et al. (2007).

2.3. Weighting

Naturally, the reliability of the hydrographic measurements used in the mixing equations depended on the hydrographic property measured. Therefore, each property's mixing equation in Eq. (4) was multiplied by a different weight, w_j ($j = 1 \ldots n_v$), prior to optimisation. The weight given to each property was calculated from the inverse of the uncertainty associated with that property, u_j (so $w_j = 1/u_j$). This minimised the residuals given by the POMP method, which were measured by the Weighted Least Squares (WLS) cost function (CF_W). This is equal to the sum of the squared residuals (the difference between the model and the measurements) weighted by w_j:

$$CF_W = \sum_{k=1}^{N} \sum_{j=1}^{n_v} \left(w_j \left(\boldsymbol{S_j C B_k^T} - \boldsymbol{Y_{jk}} \right) \right)^2 = \sum_{k=1}^{N} \sum_{j=1}^{n_v} \left(\frac{\boldsymbol{S_j C B_k^T} - \boldsymbol{Y_{jk}}}{u_j} \right)^2, \tag{5}$$

where w_j is the weight applied to the jth hydrographic property, u_j is the uncertainty in the jth hydrographic property, $\boldsymbol{S_j}$ is the jth row of $\boldsymbol{S}$ and $\boldsymbol{B_k}$ is the kth row of $\boldsymbol{B}$.

The uncertainty in each property, u_j, is equal to the measurement error plus the environmental variability. The observed environmental variability, however, is usually far more significant, due to the influence of seasonal and inter-annual variability. The environmental variability of a property was taken as the standard deviation in that property, s_j. To calculate the standard deviation, replicate samples would ideally have been taken across both the FIM and NOL sections. However, no replicate samples were available and a different approach had to be taken. We made the assumption that within a water mass, variability is mainly due to environmental effects. Thus, we calculated the standard deviation of each property in each water mass and then took an average standard deviation of each property across all of the water masses. As the data resolution for an individual cruise was limited (see dots in Fig. 3), using data from only May 2013 may not have adequately captured the standard deviation in each property. Therefore, this procedure was applied individually to each set of data collected in May over the period 2009–2013. The standard deviation in each property was then taken from the year yielding the maximum standard deviation in that property. We acknowledge that this method is an over-simplification because the standard deviations will have been influenced by mixing, but at least this method over-estimates the uncertainties, which is preferable to under-estimation.

For the temperature, salinity and nutrient measurements, the uncertainties due to environmental variability were significantly higher than the measurement uncertainty and, therefore, the latter were neglected. The uncertainties associated with the triplicate $\delta^{18}O$ measurements, while relatively small, were of a comparable magnitude to those associated with the environmental variability and, therefore, both sources of uncertainty were taken into account. The total uncertainties are summarised in Table 1.

2.4. Selection of spline function complexity

Before the mixing fractions were calculated, we had to select a suitable spline function complexity, which is similar to choosing the resolution of a model. This complexity was determined by the number of B-spline functions in the x-direction (n_l) and in a depth direction (n_z), as well as their order in each direction (k_l, k_z). To determine the optimum complexity, we followed the method of de Brauwere (2007) and systematically increased (n_l, n_z); for each (n_l, n_z) combination, we then found the (k_l, k_z) combination that minimised CF_W. The optimum complexity was taken as the (n_l, n_z) combination that gave a relatively steep reduction in the cost function for a small increase in (n_l, n_z). However, de Brauwere et al. (2007) also suggest considering the scale of the features you wish to resolve when choosing the complexity; we were interested in resolving all of the water masses. While the objective method described above suggested a value of n_z=3 on the NOL section, this was not adequate enough to resolve the MEIW, which is thinner in the vertical in the north of the channel where it has mixed less than in the south. All values of $n_z \geq 4$, however, did resolve the MEIW on the NOL section, so the lowest of these was chosen, n_z=4.

2.5. Definition of Source Water Types (SWTs)

Recall that to solve the mixing equations, we need to define a set of characteristic hydrographic properties for each water mass; these are known as the source water types (SWTs) (Tomczak, 1999). Determining the SWTs is one of the most important parts of POMP analysis, as the final mixing fractions are highly sensitive to the decisions made (de Brauwere et al., 2007). Thus, considerable attention was paid to this part of the process.

To define the SWTs, we used data from the field area rather than the water mass source regions, in accord with de Brauwere et al. (2007). It did not seem sensible to use source region data because of the effects of mixing in transit towards the FSC and, additionally, the non-conservative nature of nutrients over large areas of the ocean (Poole and Tomczak, 1999). Mixing within the FSC did make it difficult to isolate the water masses in their purest form, but this problem was minimised by using water mass properties on the boundaries of the field area. Thus, bearing in mind that the FIM section lies to the south of the NOL section, for the inflow (northward flowing – NAW), FIM data was used, whereas for the outflow (southward flowing – MNAW, MEIW, NSAIW and NSDW), NOL data was used. Due to limited $\delta^{18}O$ data resolution, exceptions had to be made for the $\delta^{18}O$ properties of

the MEIW, NSAIW and NSDW SWTs: these were defined using both NOL and FIM data. Furthermore, we used all the available FSC section data from the period May 2009 – May 2013, rather than restricting it to the period we performed the POMP analysis for (i.e. May 2013). This decision was made to minimise potential biases due to annual and seasonal variability in the channel. For example, the May 2013 temperature and salinity measurements (see Fig. S2 in the Supplementary Items) suggested that MEIW was either very weak that year, or not present in the channel: this was manifested in a small degree of convexity in the T–S diagram. Historically, MEIW has been observed to a better degree by Borenäs et al. (2001). Thus, it was not appropriate to use only the May 2013 data to characterise the SWT properties of MEIW.

The characteristic temperatures and salinities of the water masses in the FSC are well documented and are usually defined by identifying prominent end members in T–S diagrams (Turrell et al., 1999; Hansen and Østerhus, 2000; Borenäs et al., 2001). Adopting this approach defines T and S SWT properties that represent the water masses in their purest form and, thus, minimises the influence of mixing. The nutrient and $\delta^{18}O$ SWTs proved far more difficult to define than the T and S SWTs, because the nutrient and $\delta^{18}O$ contents of the FSC water masses are not yet well established. Therefore, a few definition methods were tested to find the optimum solution. This optimum method was defined by the solution that minimised CF_W. We found that the optimum method was actually the simplest approach, where we chose the nutrient and $\delta^{18}O$ values that corresponded to the T and S SWTs. To ensure consistency between the T–S SWTs, and nutrient and $\delta^{18}O$ SWTs, we chose to use the lower resolution water sample data to define the T and S rather than the high resolution CTD data. An explanation of how the SWTs were defined will now follow.

The NAW is highly saline in its purest form in the FSC and its SWTs were represented by the data-point with the maximum salinity on the east side of the FIM section (FIM01 – FIM03), at or below a depth of 50 m, as suggested by Hughes et al. (2006). This depth restriction was used to minimise the stronger influence of seasonality on the nutrient data that occurs in surface waters. Similarly, the MNAW was identified by the maximum salinity on the west side of the NOL section (NOL08 – NOL11), also at or below a depth of 50 m. The MEIW and NSAIW were both defined by the minimum salinities within their standard salinity and temperature ranges published in the literature (Borenäs et al., 2001). Unfortunately, the resolution of the water sample data was not high enough to capture the MEIW's salinity minimum; thus, an exception was made and the higher resolution CTD data was used to define the MEIW's T and S SWTs. Finally, the NSDW is the deepest water mass and its T and S SWTs were therefore defined by the data point with the maximum density. In all cases, the SWTs were calculated for each month available between May 2009 – May 2013, and the median values were used as the final SWTs. To ensure the SWTs were realistic, we checked that they were within or similar to standard ranges/values published in the literature or in databases; the SWTs were found to be in general agreement. Table 1 summarises the SWTs and available literature/database values.

2.6. Uncertainties

The mixing fractions calculated by POMP analysis only represent one solution to the problem and do not take into account uncertainties due to environmental variability (de Brauwere et al., 2007). For example, the fractions might have a low cost function, but if this is due to over-fitting they will be very sensitive to perturbations and, therefore, will be associated with a relatively high uncertainty. Thus, we ran a number of Monte-Carlo simulations, which perturbed the observations with random noise (within the limits of the uncertainties used in the weighting scheme). One thousand simulations were performed in three separate cases, on both FIM and NOL for the first case and on FIM only for the last two cases: (1) without $\delta^{18}O$ and with the full nutrient dataset; (2) without $\delta^{18}O$ and with nutrient data, but only using nutrients where there were $\delta^{18}O$ measurements; and (3) with $\delta^{18}O$ and nutrient data. By doing this, our aim was to objectively determine the optimum data combination for performing POMP analysis in the FSC.

3. Results and discussion

3.1. $\delta^{18}O$ and nutrient SWTs

Fig. 2 shows the $\delta^{18}O$ and nutrient concentrations within each water mass for all observations between May 2009 and May 2013 (where the data was filtered based on the T and S literature SWTs in Table 1). They indicate that each water mass has a distinct range of $\delta^{18}O$ and nutrient values, which agree well with the literature and database values (Table 1); thus, this validates our use of $\delta^{18}O$ and nutrients as tracers of the FSC water masses in the POMP analysis. T–S plots coloured by observed nutrient and $\delta^{18}O$ observations collected between May 2009 and May 2013 show similar distinct ranges by water mass (Fig. S2). The nutrient ranges for each water mass are quite large, but this is likely a reflection of our use of data from different months and, hence, seasonal variability.

3.2. POMP summary statistics

The summary statistics of the POMP analysis for each case tested are summarised in Tables 2 and 3 below. The residual degrees of freedom (DF) have been given to provide a means of comparing CF_W for each case. As CF_W is weighted, it is dimensionless and, therefore, CF_W should approximate DF. Hence a CF_W that is larger in magnitude than DF suggests the presence of model errors, such as errors in the SWTs or errors due to non-conservation (de Brauwere, 2007). Comparing CF_W relative to DF and the uncertainties for each case reveals that, at present, using only nutrients and no $\delta^{18}O$ data (case one) delivers the best results. CF_W is noticeably higher on NOL than on FIM, and may reflect larger environmental variability (in particular the range of temperature residuals is greater on NOL than on FIM Figs. 4 and 5). On the NOL section, CF_W is also slightly larger than DF; although this could potentially suggest model errors, the uncertainty estimates (Table 3) are very similar to those on the FIM section.

However, it is not surprising that case one delivered the best results, because the $\delta^{18}O$ FIM dataset only consisted of 24 datapoints, whereas the nutrient FIM dataset consisted of 93 datapoints. A comparison of cases two and three shows that when the resolution of the nutrient dataset is reduced to the resolution of the $\delta^{18}O$ dataset, the addition of $\delta^{18}O$ does improve the results: in case two, CF_W is higher than DF, and in case three, CF_W is lower than DF. Furthermore, the uncertainties associated with the NAW and MNAW mixing fractions are also slightly reduced (Table 3).

Notice that in all cases, the NAW and MNAW uncertainties are higher than those associated with the intermediate and deep waters. This probably reflects the fact that the characteristics of the NAW and MNAW, as upper layer water masses, are more variable over different months and years.

3.3. Water mass distributions

The mixing fractions calculated for the optimum case (case one) are shown in Fig. 3 for both sections. Fig. S1 in the

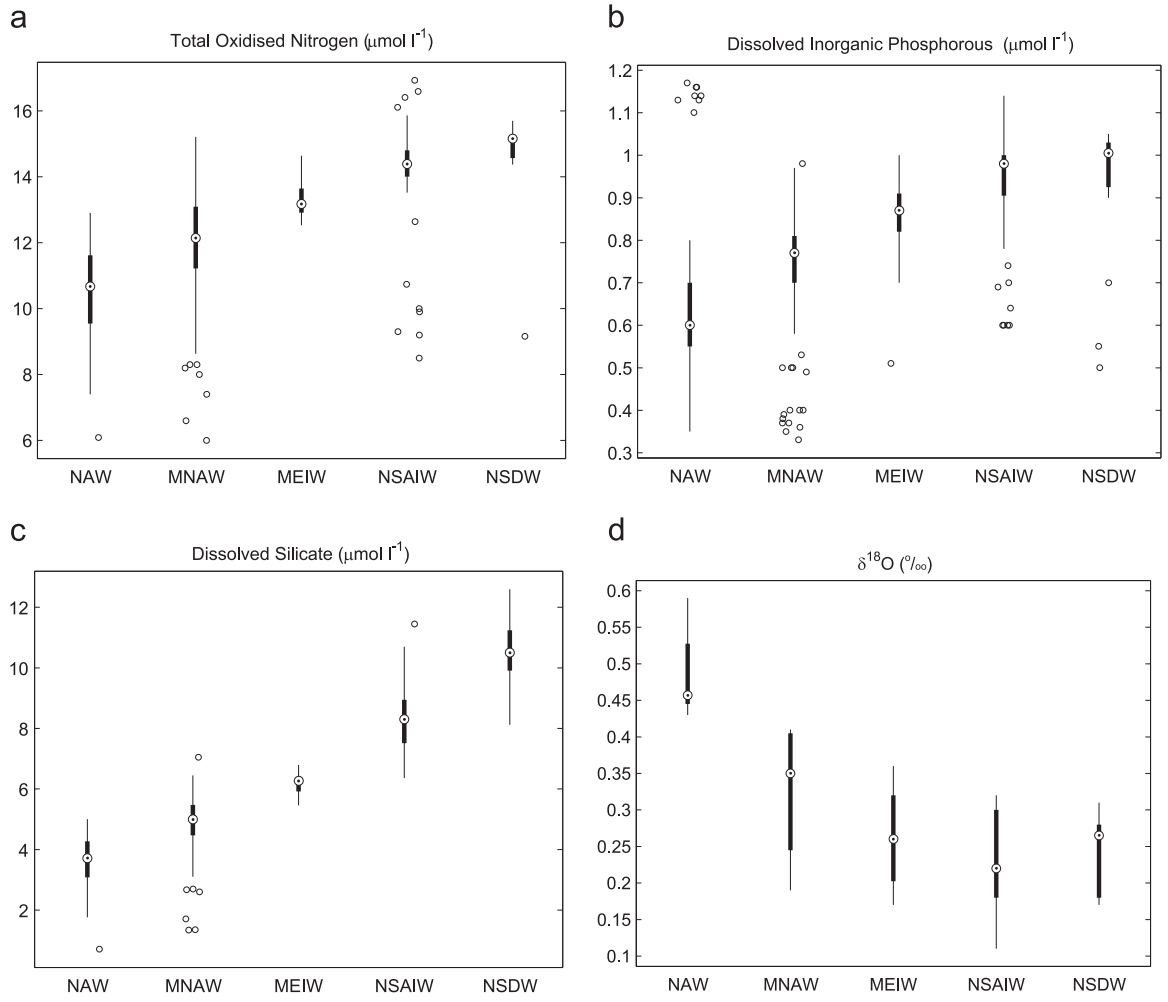

Fig. 2. Boxplot of Total Oxidised Nitrogen, Dissolved Inorganic Phosphorous, Dissolved Silicate concentrations and $\delta^{18}O$ per water mass, from observations between May 2009 and May 2013 (where the data was filtered based on the T and S literature SWTs in Table 1). Boxplots show the median (middle circle), the .25 and .75 quantile (thick line), the range of values not considered as outliers (thin line), and outliers (open circles; defined as outside 1.5 times the .25 and .75 inter-quantile range).

Table 2
Weighted Least Squares cost function (CF_W) and degrees of freedom (DF) for all three cases tested from the best POMP analysis.

Method	FIM		NOL	
	CF_W	**DF**	**CF_W**	**DF**
(i) No $\delta^{18}O$, all nutrients	142.74	405	455.09	352
(ii) No $\delta^{18}O$, limited nutrients	91.05	88	–	–
(iii) With $\delta^{18}O$, limited nutrients	102.71	112	–	–

Supplementary materials shows case three's mixing fractions on the FIM section, while case two is not included because the fractions were very similar to case three's.

All five water masses are present on both sections and occupy the general areas that we would expect from past studies (Turrell et al., 1999; Hansen and Østerhus, 2000). For comparison, mixing fractions as calculated by a three-point mixing model (Hermann, 1967) on both sections are shown in Fig. 6. Below, we will discuss the results of the estimated water mass distributions in greater detail, highlighting the benefits of POMP over the more traditional three-point mixing model.

In general, the residuals from POMP associated with the mixing fractions are approximately normally distributed and centred about zero for both sections (Figs. 4 and 5). This suggests that residual variability is due to stochastic errors rather than errors in the SWTs or non-conservative behaviour. The relatively small number of observations remains an issue, even in case one which has the largest density of observations across the section. The phosphate residuals are systematically too positive in the regions

Table 3
Uncertainties associated with the mixing fractions (in %) for each case tested determined from 1000 Monte-Carlo simulations perturbed with random noise (within the limits of the uncertainties).

Method	FIM					NOL				
	NAW	**MNAW**	**MEIW**	**NSAIW**	**NSDW**	**NAW**	**MNAW**	**MEIW**	**NSAIW**	**NSDW**
(1) No $\delta^{18}O$, all nutrients	5.2	7.0	3.9	5.0	4.6	5.3	7.1	3.1	4.2	3.6
(2) No $\delta^{18}O$, limited nutrients	8.5	11.0	3.9	5.6	5.9	–	–	–	–	–
(3) With $\delta^{18}O$, limited nutrients	8.1	10.6	3.9	5.6	5.9	–	–	–	–	–

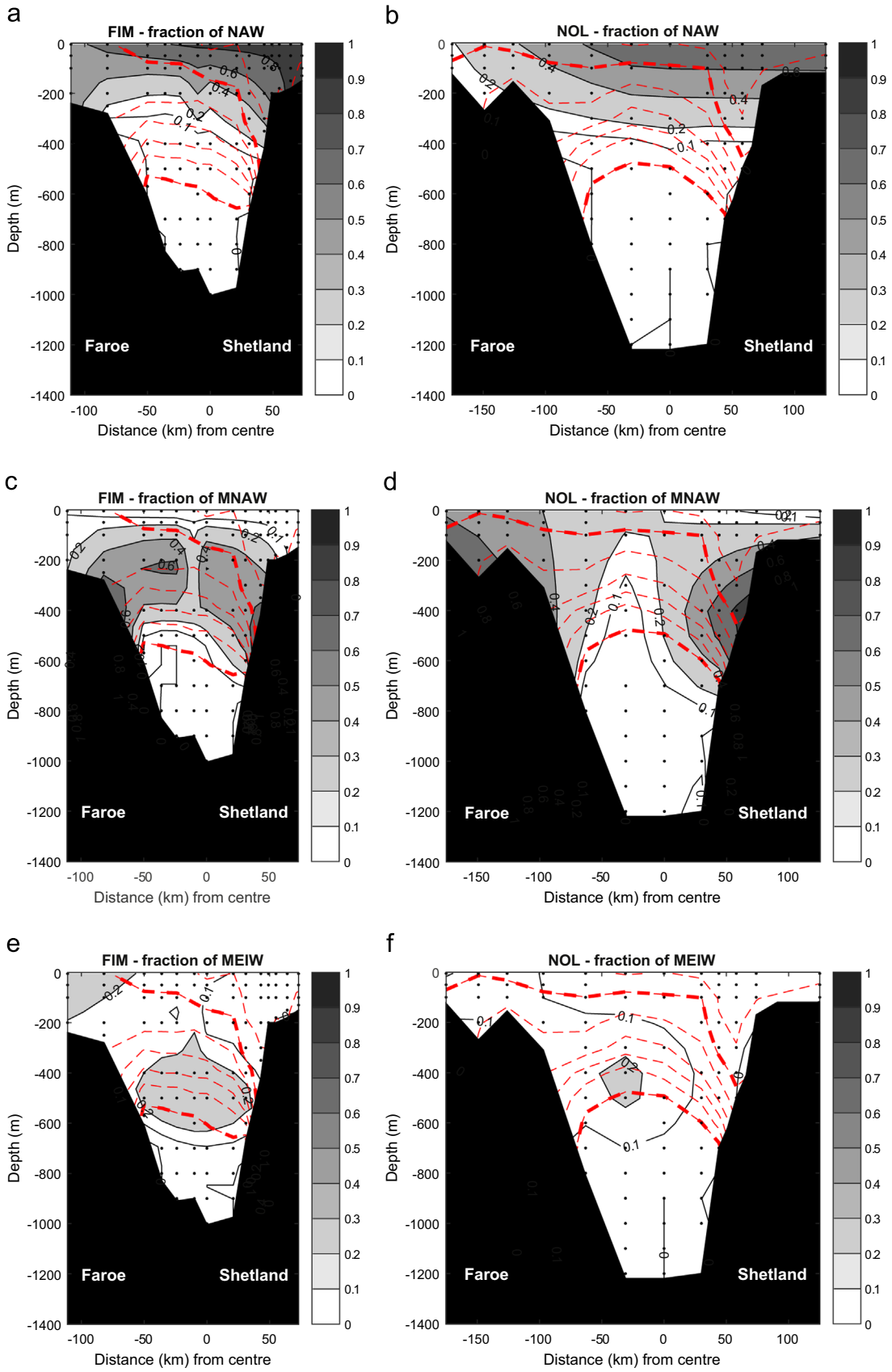

Fig. 3. Mixing fractions estimated using POMP in May 2013 on the FIM (left) and NOL (right) section, using the SWTs defined in Table 1. The red dashed contours are isopycnals (potential density in kg m^{-3}) and range from 27.4 (near the surface) to 28.0 (at the bottom), in increments of 0.1 kg m^{-3} (27.5 and 28.0 kg m^{-3} isopycnals in bold). The small grey dots indicate the measurement depths.

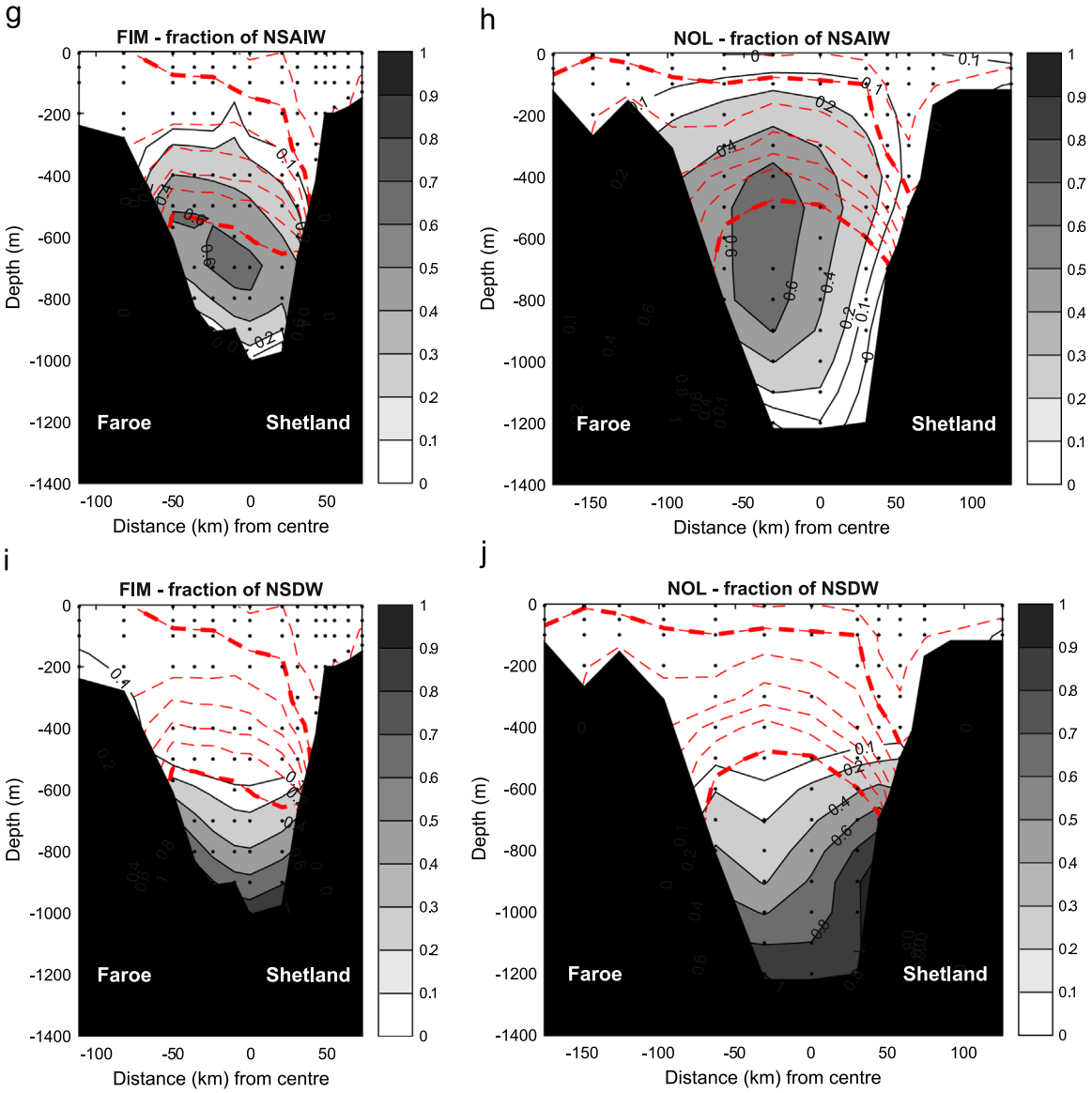

Fig. 3. (*continued*)

occupied by MNAW and NAW on FIM (not shown). This may be due to non-conservative effects in the surface layer. These non-conservative effects only seem to be obvious in surface waters where phosphate and nitrate are depleted.

3.3.1. Atlantic Water Masses (NAW/MNAW)

Particularly noticeable is the interesting geometry of the MNAW on each section (Fig. 3c and d), which indicates a re-circulation of the MNAW south of the FIM section, as is widely suggested in the literature (Dooley and Meincke, 1981; van Aken, 1988; Sherwin et al., 1999; Sherwin et al., 2008b). At the NOL section, the MNAW distribution suggests a pathway across the Faroese shelf, while at the FIM section this water mass is much more topographically steered at the Faroese shelf edge and occupies a wider area across the FSC. Furthermore, despite the complex mixing pattern this causes between MNAW and NAW, coupled with their similar origins and characteristics, POMP still differentiates well between these two Atlantic water masses.

NAW occupies most of the surface waters across both sections (Fig. 3a and b), more so than previously determined (Hughes et al., 2006). As seasonal stratification occurs across the FSC, warmer surface temperatures and reduced nutrient concentrations (due to primary productivity) in this surface layer may cause MNAW at the Faroese edge of the FSC (normally cooler and more enriched in nutrients; Fig. 2) to be represented as NAW in the POMP analysis.

For comparison, Fig. 6 shows the distribution of the Atlantic water mass as determined by a three-point mixing model. Because such an approach is limited to representing only three water masses, it cannot distinguish between MNAW and NAW and, therefore, misses the MNAW's recirculation. This immediately highlights one significant benefit of using POMP in the FSC.

3.3.2. Intermediate Water Masses (MEIW)

POMP performs less well in differentiating MEIW from the overlying MNAW and the underlying NSAIW. This is particularly noticeable in Fig. 3e, where MEIW is found in the surface waters on the west side of the section, cut-off from the mid-water layer. This is not surprising as MEIW is partly composed of MNAW (Hansen and Østerhus, 2000) and, therefore, may have some similar properties to the MNAW. Indeed, Fig. 2 shows that MEIW's nutrient range is very similar to the upper nutrient range of the MNAW and they also have very similar $\delta^{18}O$ ranges. Thus, the MEIW is probably particularly complex and challenging to represent.

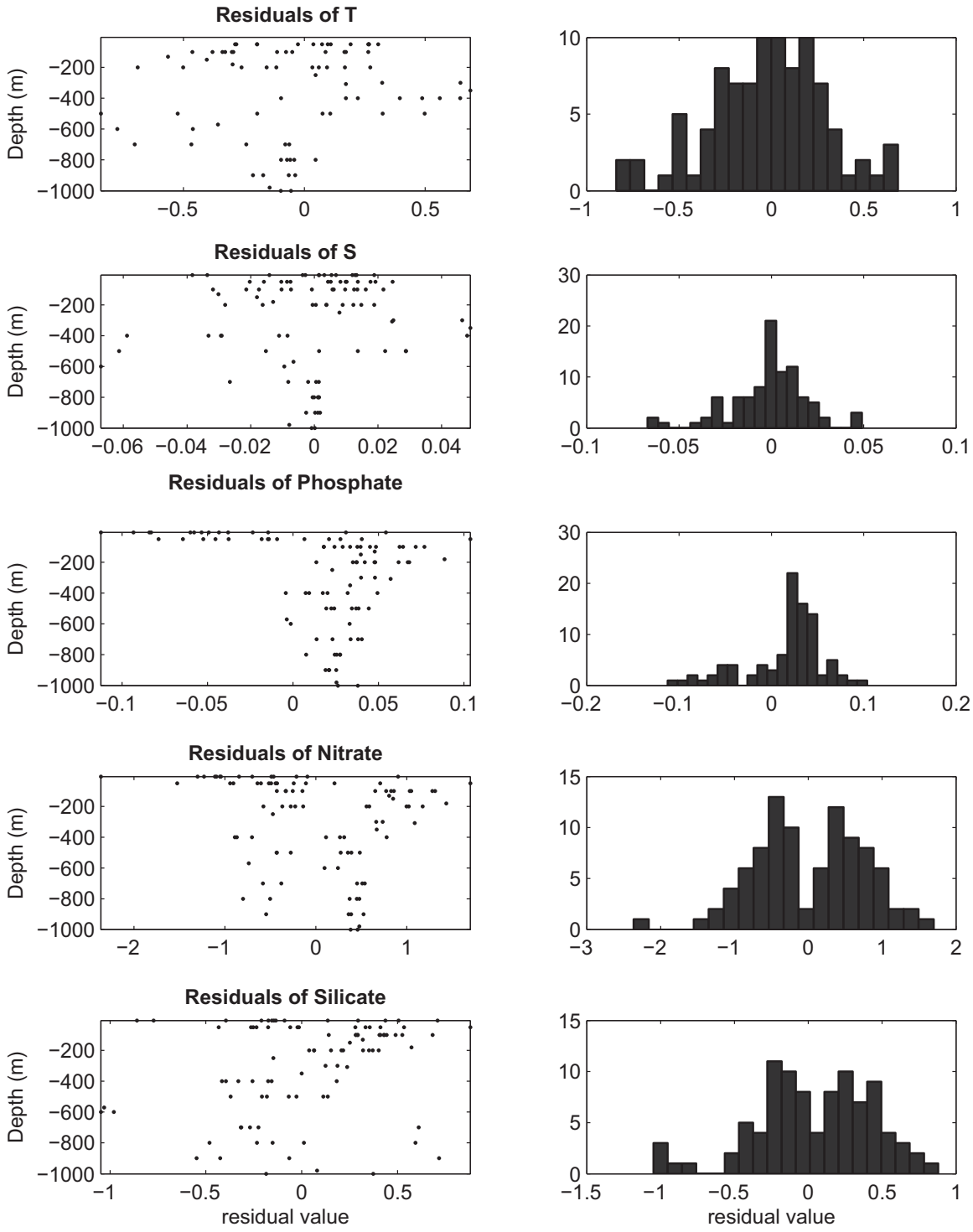

Fig. 4. Residuals for each of the parameters (temperature, salinity, phosphate, nitrate and silicate) of the POMP analysis for the FIM section observations from May 2013. Left-side panels show the residuals with depth, while right-side panels show histograms of the residuals.

Or, perhaps the difficulty with the MEIW arose because it was not present in the FSC in May 2013. Previous researchers have commented on the transient nature of MEIW in the FSC (Borenäs et al., 2001), and an investigation in T–S space does suggest only a small degree of convexity in May 2013 (especially in comparison with their Fig. 3). However, although omission of MEIW from the POMP analysis does not significantly influence the distribution of the 4 remaining water masses (not shown), it does increase the residuals of the POMP analysis. The additional DF due to a reduced set of estimated parameters in the POMP analysis are not sufficient to compensate for this increase in CF_W, confirming MEIW should be considered as part of water mass analysis in the region.

The three-point mixing model (Fig. 6c and d) shows more promise in distinguishing the intermediate water mass at depth on both sections. However, results from the NOL section (Fig. 6d) also identify the intermediate water mass in the surface layers of the Faroese shelf, similar to the POMP analysis.

3.3.3. *Norwegian Sea Water Masses (NSAIW/NSDW)*

The NSAIW distribution calculated by POMP analysis (Fig. 3g

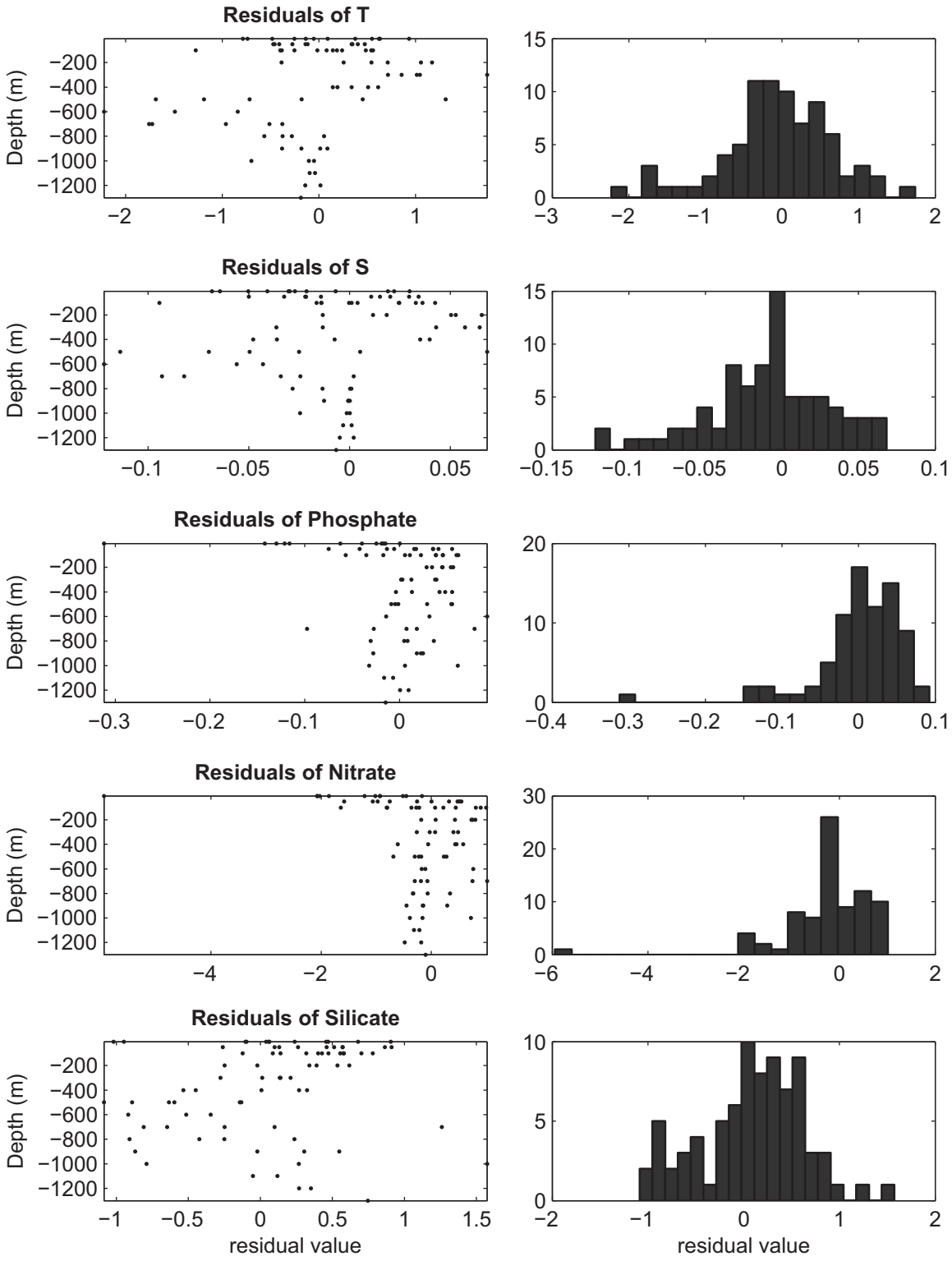

Fig. 5. Residuals for each of the parameters (temperature, salinity, phosphate, nitrate and silicate) of the POMP analysis for the NOL section observations from May 2013. Left-side panels show the residuals with depth, while right-side panels show histograms of the residuals.

and h) is consistent with the accepted literature and suggests a pathway in the FSC where the currents enter the channel on the western side, and spread laterally as they flow south-westward. The core of NSAIW also reduces in size and its distribution shifts deeper in isopycnal space, a strong indication of mixing with the underlying NSDW. NSDW in the FSC is confined on both sections to the deepest parts (Fig. 3i and j). Its distribution on the NOL section suggests a pathway hugging the Shetland shelf edge.

Comparison with results from the three-point mixing model (Fig. 6) again highlights the strength of POMP analysis to distinguish all 5 water masses in the FSC. The results from POMP are the first to separate the deep waters of the FSC into its two water masses, NSAIW and NSDW.

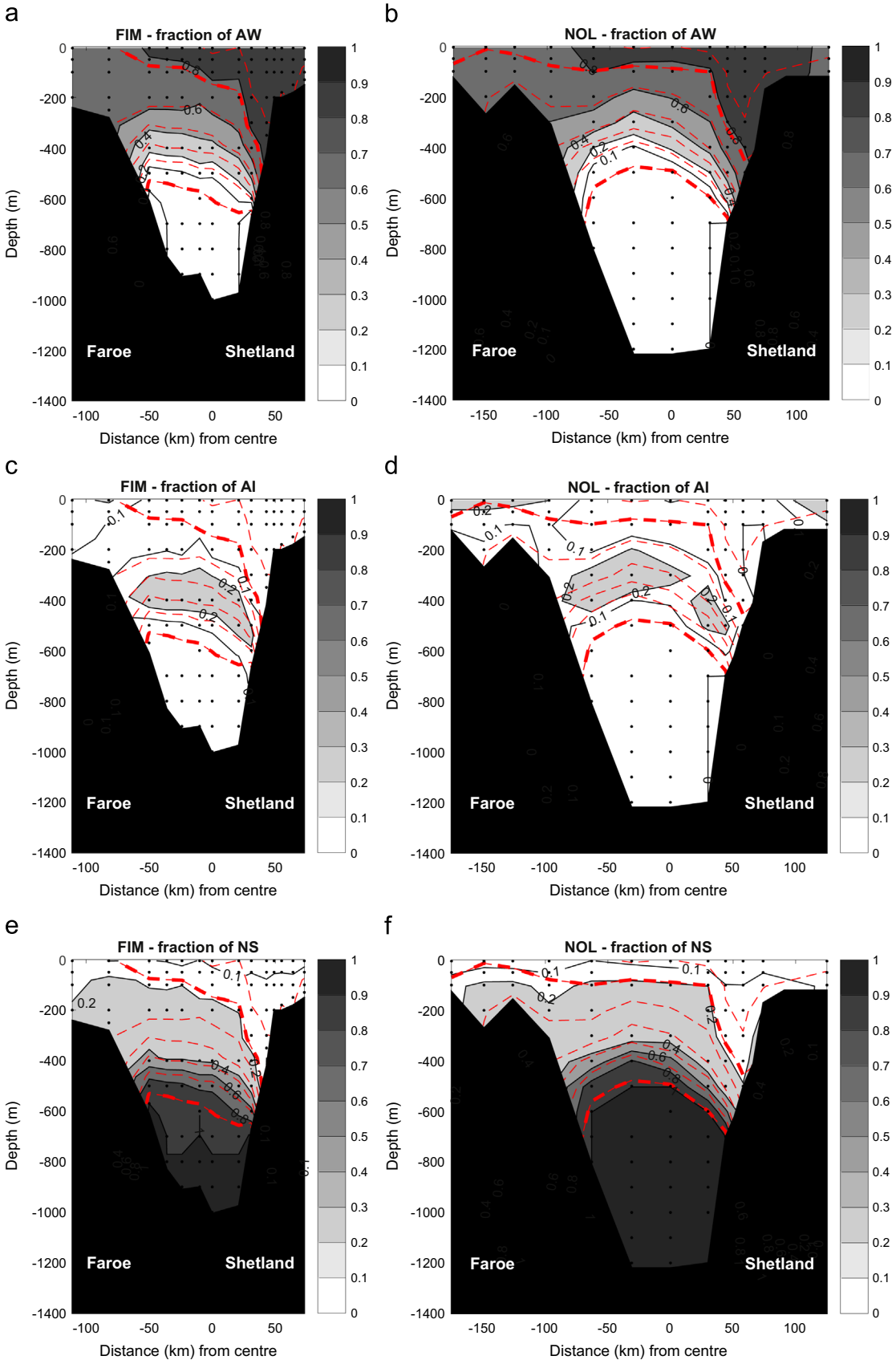

Fig. 6. Mixing fractions estimated using three-point mixing model in May 2013 on the FIM (left) and NOL (right) section (see text for details). The red dashed contours are isopycnals (potential density in kg m^{-3}) and range from 27.4 (near the surface) to 28.0 (at the bottom), in increments of 0.1 kg m^{-3} (27.5 and 28.0 kg m^{-3} isopycnals in bold). The small grey dots indicate the measurement depths.

3.3.4. Decomposition of volume transport by water mass

The volume transport based on the calculated geostrophic velocities on both FIM and NOL sections in the FSC has been widely presented in the literature previously (Tait, 1957; Dooley and Meincke, 1981; van Aken, 1988; Sherwin et al., 1999, 2008b; Hughes et al., 2006; Berx et al., 2013). The water mass fractions determined by POMP analysis provide an opportunity to decompose this transport by water mass. To achieve this, we calculated the geostrophic velocities from the observed CTD profiles along the FIM and NOL section in May 2013, using the dynamic method (see Pond and Pickard, 1983). The bottom triangle adjustment was calculated through interpolation on density surfaces.

In order to convert these geostrophic velocity shear profiles to absolute geostrophic velocities, a level of no motion needs to be assumed or velocities at a reference level need to be known. Berx et al. (2013) demonstrated the benefits of incorporating altimetry observations in the FSC, and, here, we have used the surface geostrophic velocities produced by Ssalto/Duacs and distributed by Aviso, with support from Cnes (http://www.aviso.oceanobs.com/duacs/) as a reference. Although our estimates are consistent between the two sections, they are lower than previously published transport estimates. This could be due to natural variability (our values are within the range of published variability), or possibly due to a need to further refine the methodology to estimate the velocity field from hydrography. However, we argue that using POMP to achieve the decomposition by water mass is novel and deserves to be included here, while a more detailed review of the methodology to calculate volume, heat and salt transport warrants presentation on its own, and is beyond the scope of this paper.

Volume transport was calculated by multiplying the geostrophic velocities with their associated area (defined as the bin size of the CTD data multiplied by the distance between the midpoints of the CTD profiles) and integrating from surface to sea bed and between the 200 m contours on the edges of the FSC (in part to avoid inclusion of the large areas of shallow shelf which are sampled at NOL but not at FIM). To decompose the transport by water mass, POMP fractions were interpolated and included as a multiplier prior to integration. An overview of the net volume transports obtained in this manner is presented in Table 4.

The calculated volume transports, as one might expect, are consistent between the two sections and, once again, the decomposition by water mass demonstrates the strength of POMP analysis. Table 4 shows that the intermediate waters of the FSC show very little net transport across either of the sections. The division of the Atlantic water masses shows a relatively small and positive contribution of MNAW. The lack of MNAW in the surface waters on the Faroese edge of the channel (Fig. 3) could mean this is an underestimate, however. The volume transport of the water masses of Norwegian Sea origin (NSAIW and NSDW) is approximately equally split; suggesting NSAIW is a more significant contributor to the overflow waters than previously reported. Further investigations are planned to provide error estimates on these volume transports and study their variability in time.

Table 4
Net volume transport (in Sv; 1 Sv = 10^6 m^3 s^{-1}) on the FIM and NOL section through the FSC, decomposed into different water masses using fractions determined by POMP analysis (NAW = North Atlantic Water; MNAW = Modified North Atlantic Water; MEIW = Modified East Icelandic Water; NSAIW = Norwegian Sea Arctic Intermediate Water; NSDW = Norwegian Sea Deep Water). Positive transports are directed towards the Nordic Seas, negative ones towards the Atlantic.

	FIM	NOL
Total	1.05	1.14
NAW	1.22	1.06
MNAW	0.31	0.59
MEIW	−0.01	0.01
NSAIW	−0.24	−0.21
NSDW	−0.26	−0.35

4. Conclusions

We applied POMP analysis (de Brauwere et al., 2007) to observations of temperature, salinity, nutrient concentrations and $\delta^{18}O$ in the Faroe-Shetland Channel in May 2013. The observations of $\delta^{18}O$ are of particular interest as they are the first observations collected in this region (Schmidt et al., 1999).

Despite the potential inaccuracies in the POMP analysis, discussed above, the method produces water mass distributions consistent with our current knowledge of circulation in the FSC (Turrell et al., 1999; Hansen and Østerhus, 2000). Our results in particular highlight the recirculation of MNAW in the FSC and small differences in the pathways of the two deepest water masses (NSAIW and NSDW). Also, the NAW's core is concentrated on the Shetland slope at FIM, while at NOL the core appears to have spread out into the channel; this seems realistic, because the NAW gradually mixes with the MNAW as it flows northwards. Additionally, the overflow water masses spread out and sink as they move southwards through the channel, reflecting vertical and lateral mixing between the warmer, more saline MNAW; the cooler, fresher intermediate waters; and the cold, dense deep waters. We demonstrate the potential application of POMP to decompose the volume transport through the FSC by water mass, highlighting the contribution of MNAW in the surface, Atlantic-origin layer and the equal contribution of NSAIW and NSDW to the deep overflow waters.

This work highlights the need for improved spatio-temporal resolution of the data, and coincident observations of all parameters for best estimates of the mixing fractions of the 5 main water masses in the FSC. $\delta^{18}O$ observations, in particular, could provide an additional parameter in constraining the POMP analysis, thereby potentially reducing uncertainty in the results.

Acknowledgements

This work received funding from the MASTS pooling initiative (The Marine Alliance for Science and Technology for Scotland) and their support is gratefully acknowledged. MASTS is funded by the Scottish Funding Council (grant reference HR09011) and contributing institutions. The research leading to these results has received funding from NACLIM, a project of the European Union 7th Framework Programme (FP7 2007–2013) under Grant agreement no. 30829. Salinity analyses were conducted by members of the Oceanography Group at Marine Scotland Science: we would like to thank David Lee, Matthew Geldart, Dougal Lichtman and George Slesser for their efforts. Nutrient analyses were performed by the Analytical Chemistry Group at Marine Scotland Science: we are grateful to Pamela Walsham, Alison Taylor and Lynda Webster. Oxygen isotope analyses were conducted by WENA and Angus Calder at the University of St Andrews; we acknowledge helpful discussions of these data with Lauren Gillespie. The POMP analysis computer code was kindly given to us by Anouk de Brauwere, for which we are very grateful.

Appendix A. Supplementary material

Supplementary data associated with this article can be found in the online version at http://dx.doi.org/10.1016/j.dsr.2015.10.013.

References

Armstrong, F.A.J., Stearns, C.R., Strickland, J.D.H., 1967. The measurement of upwelling and subsequent biological processes by means of the Technicon AutoAnalyzer and associated equipment. Deep. Sea Res. 14 (3), 381–389.

Austin, W.E.N., Inall, M.E., 2002. Deep-water renewal in a Scottish fjord: temperature, salinity and oxygen isotopes. Polar Research 21 (2), 251–257.

Berx, B., Hansen, B., Østerhus, S., Larsen, K.M., Sherwin, T., Jochumsen, K., 2013. Combining in situ measurements and altimetry to estimate volume, heat and salt transport variability through the Faroe-Shetland Channel. Ocean Sci. 9, 639–654 10.5194/os-9-639-2013.

Borenäs, K.M., Lake, I.L., Lundberg, P.A., 2001. On the intermediate water masses of the Faroe-Bank Channel Overflow. J. Phys. Ocean. 31 (7), 1904–1914.

de Brauwere, A., Jacquet, S.H., De Ridder, F., Dehairs, F., Pintelon, R., Schoukens, J., Baeyens, W., 2007. Water mass distributions in the Southern Ocean derived from a parametric analysis of mixing water masses. J. Geophys. Res.: Ocean. (1978–2012) 112 (C2).

de Brauwere, A., Jacquet, S.H.M., De Ridder, F., Dehairs, F., Pintelon, R., Schoukens, J., Baeyens, W., 2007. Water mass distributions in the Southern Ocean derived from a parametric analysis of mixing water masses. J. Geophys. Res. 112, C02021 10.1029/2006JC003742.

Dickson, H.N., 1903. The Hydrography of the Faeroe-Shetland Channel. Geogr. J. 21 (4), 418–436.

Dickson, R.R., Meincke, J., Malmberg, S.A., Lee, A.J, 1988. The "Great Salinity Anomaly" in the northern North Atlantic 1968-1982. Progress in Oceanography 20, 103–151.

Dooley, H.D., Meincke, J., 1981. Circulation and water masses in the Faroese Channels during Overflow '73. Dtsch. Hydrogr. Z. 34 (2), 41–55.

Frew, R.D., Dennis, P.F., Heywood, K.J., Meredith, M.P., Boswell, S.M., 2000. The oxygen isotope composition of water masses in the northern North Atlantic. Deep-Sea Res. Part I: Ocean. Res. Pap. 47 (12), 2265–2286.

Garcia, H.E., Locarnini, R.A., Boyer, T.P., Antonov, J.I., Baranova, O.K., Zweng, M.M., Reagan, J.R., & Johnson, D.R. (2014). *World Ocean Atlas 2013, Volume 4: Dissolved Inorganic Nutrients (phosphate, nitrate, silicate)*. S. Levitus, Ed., A. Mishonov Technical Ed.; NOAA Atlas NESDIS 76, 25pp.

Gregory, J.M., Dixon, K.W., Stouffer, R.J., Weaver, A.J., Driesschaert, E., Eby, M., Fichefet, T., Hasumi, H., Hu, A., Jungclaus, J.H., Kamenkovich, I.V., Levermann, A., Montoya, M., Murakami, S., Nawrath, S., Oka, A., Sokolov, A.P., Thorpe, R.B., 2005. A model intercomparison of changes in the Atlantic thermohaline circulation in response to increasing atmospheric CO_2 concentration. Geophys. Res. Lett. 32, 12.

Hall, R.A., Huthnance, J.M., Williams, R.G., 2011. Internal tides, nonlinear internal wave trains, and mixing in the Faroe-Shetland Channel. J. Geophys. Res. 116, C03008 10.1029/2010JC006213.

Hansen, B., Østerhus, S., 2000. North Atlantic-Nordic Seas exchanges. Prog. Oceanogr. 45 (2), 109–208.

Hansen, B., Østerhus, S., Hátún, H., Kristiansen, R., Larsen, K.M.H., 2003. The Iceland-Faroe inflow of Atlantic water to the Nordic Seas. Prog. Oceanogr. 59 (4), 443–474.

Hansen, B., Østerhus, S., 2007. Faroe Bank Channel overflow 1995–2005. Prog. Oceanogr. 75 (4), 817–856.

Hermann, F., 1967. The TS Diagram Analysis of the Water Masses over the Iceland-Faroe Ridge and in the Faroe Bank Channel (Overflow '60). Rapports et Procès-Verbaux des Réunions du Conseil International pour l'Exploration de la Mer, vol. 157, pp.139–149.

Hosegood, P., van Haren, H., 2004. Near-bed solibores over the continental slope in the Faeroe-Shetland Channel. Deep. Sea Res. Part II: Top. Stud. Oceanogr. 51 (25), 2943–2971.

Hosegood, P., van Haren, H., Veth, C., 2005. Mixing within the interior of the Faeroe-Shetland Channel. J. Mar. Res. 63 (3), 529–561.

Hughes, S.L., Turrell, W.R., Hansen, B., Østerhus, S., 2006. Fluxes of Atlantic Water (volume, heat and salt) in the Faroe-Shetland Channel Calculated from a Decade of Acoustic Doppler Current Profiler data (1994–2005), Fisheries Research Services Collaborative Report, (01/06).

Johnson, C., Inall, M., Häkkinen, S., 2013. Declining nutrient concentrations in the northeast Atlantic as a result of a weakening Subpolar Gyre. Deep. Sea Res. Part I: Oceanogr. Res. Pap. 82, 95–107.

Klein, B., Tomczak, M., 1994. Identification of diapycnal mixing through optimum multiparameter analysis: 2. Evidence for unidirectional diapycnal mixing in the front between North and South Atlantic Central Water. J. Geophys. Res.: Ocean. (1978–2012) 99 (C12), 25275–25280.

Koroleff, F., 1971/C. On the determination of reactive silicate in natural waters ICES C.M., p. 43.

Larqué, L., Maamaatuaiahutapu, K., Garçon, V., 1997. On the intermediate and deep water flows in the South Atlantic Ocean. J. Geophys. Res.: Ocean (1978–2012) 102 (C6), 12425–12440.

Larsen, K.M.H., Hátún, H., Hansen, B., Kristiansen, R., 2012. Atlantic water in the Faroe area: sources and variability. ICES J. Mar. Sci. 69 (5), 802–808.

Maamaatuaiahutapu, K., Garcon, V.C., Provost, C., Boulahdid, M., Bianchi, A.A., 1994. Spring and winter water mass composition in the Brazil-Malvinas Confluence. J. Mar. Res. 52 (3), 397–426.

Martin, J.H.A., 1993. Norwegian Sea intermediate water in the Faroe-Shetland Channel. ICES J. Mar. Sci. 50 (2), 195–201.

Meredith, M.P., Heywood, K.J., Frew, R.D., Dennis, P.F., 1999. Formation and circulation of the water masses between the southern Indian Ocean and Antarctica: results from $\delta^{18}O$. J. Mar. Res. 57 (3), 449–470.

Murphy, J., Riley, J.P., 1962. A modified single solution method for the determination of phosphate in natural waters. Anal. Chim. Acta 27, 31–36.

Østerhus, S., Turrell, W.R., Jónsson, S., Hansen, B., 2005. Measured volume, heat, and salt fluxes from the Atlantic to the Arctic Mediterranean. Geophys. Res. Lett. 32, 7.

Pond, S., Pickard, G.L., 1983. Introductory Dynamical Oceanography, 2nd edition. Pergamon Press, Oxford.

Poole, R., Tomczak, M., 1999. Optimum multiparameter analysis of the water mass structure in the Atlantic Ocean thermocline. Deep. Sea Res. Part I: Oceanogr. Res. Pap. 46 (11), 1895–1921.

Schmidt, G.A., Bigg, G.R., Rohling, E.J., 1999. Global Seawater Oxygen-18 Database (version 1.21). [online] Available at: ⟨http://data.giss.nasa.gov/o18data/⟩ [accessed 02.02.14].

Sherwin, T.J., Turrell, W.R., Jeans, D.R.G., Dye, S., 1999. Eddies and a mesoscale deflection of the slope current in the Faroe–Shetland Channel. Deep. Sea Res. Part I: Ocean. Res. Pap. 46 (3), 415–438.

Sherwin, T.J., Williams, M.O., Turrell, W.R., Hughes, S.L., Miller, P.I., 2006. A description and analysis of mesoscale variability in the Fa¨roe-Shetland Channel. J. Geophys. Res. 111, C03003 10.1029/2005JC002867.

Sherwin, T.J., Griffiths, C.R., Inall, M.E., Turrell, W.R., 2008a. Quantifying the overflow across the Wyville Thomson Ridge into the Rockall Trough. Deep. Sea Res. Part I: Oceanogr. Res. Pap. 55 (4), 396–404.

Sherwin, T.J., Hughes, S.L., Turrell, W.R., Hansen, B., Østerhus, S., 2008b. Wind-driven monthly variations in transport and the flow field in the Faroe–Shetland Channel. Polar Res. 27 (1), 7–22.

Tait, J.B., 1957. Hydrography of the Faroe-Shetland Channel 1927–1952. Mar. Res. Scotl. 2, 309.

Tomczak, M., Large, D.G., 1989. Optimum multiparameter analysis of mixing in the thermocline of the eastern Indian Ocean. J. Geophys. Res.: Oceanogr. (1978–2012) 94 (C11), 16141–16149.

Tomczak, M., 1999. Some historical, theoretical and applied aspects of quantitative water mass analysis. J. Mar. Res. 57 (2), 275–303.

Turrell, W.R., Slesser, G., Adams, R.D., Payne, R., Gillibrand, P.A., 1999. Decadal variability in the composition of Faroe Shetland Channel bottom water. Deep-Sea Res. Part I: Oceanogr. Res. Pap. 46 (1), 1–25.

van Aken, H.M., 1988. Transports of water masses through the Faroese Channels determined by an inverse method. Deep. Sea Res. Part A. Oceanogr. Res. Pap. 35 (4), 595–617.

van Bennekom, A.J., 1985. Dissolved silica as an indicator of Antarctic Bottom Water penetration, and the variability in the bottom layers of the Norwegian and Iceland Basins. Rit Fiskid. 9, 101–109.